Soft Matter

Cite this: *Soft Matter*, 2012, **8**, 942

www.rsc.org/softmatter

PAPER

Insertion properties of cholesteryl cyclodextrins in phospholipid membranes: a molecular study†

Martin Bauer,[ab] Thierry Charitat,[b] Christophe Fajolles,[a] Giovanna Fragneto[c] and Jean Daillant*[a]

Received 16th July 2011, Accepted 3rd October 2011
DOI: 10.1039/c1sm06346d

Amphiphilic cyclodextrins (CDs) are good candidates to functionalize natural membranes, as well as synthetic vesicles. In this paper, we fully describe and compare the insertion properties of the permethylated mono-cholesteryl α-CD (TASC) and its mono- and di-cholesteryl β-CD analogues (TBSC and TBdSC) in dipalmitoyl-L-α-phosphatidylcholine (DPPC) mono- and bi-layers as membrane models from the macroscopic to the molecular scale. By calculating the inverse compressibility moduli and free excess Gibbs energies from the Langmuir isotherms, the influence of the CD type, CD ratio and number of cholesteryl anchors on the membrane properties have been established. TBdSC, with its two cholesteryl residues, seems to be anchored best to the membrane compared to CD derivatives with only one anchor. Furthermore, TASC appears to be more firmly inserted into the membrane than TBSC. The in-plane structure is characterized by Brewster angle microscopy (BAM) at the air–water interface and atomic force microscopy (AFM) of the mono- and bi-layers deposited on mica. Depending on the compression, full miscibility of the cholesteryl CDs and the phospholipids is observed at low surface pressures and a clear demixing tendency is apparent during compression. CD-modified bilayers are stable and are subject to a gel–liquid phase transition upon heating. Due to their bulky CD moiety, the amphiphilic CDs exhibit a distinct fluidizing effect, shifting the DPPC's gel–liquid transition. The structure of the mixed TASC/DPPC mono- and bi-layers perpendicular to the surface is investigated with Ångstrom resolution by neutron reflectivity. In this way a molecular model of the insertion has been established, which suggests that the CD cavities partly protrude into the subphase, which should leave them accessible for complex formation.

1 Introduction

Cyclodextrins (CDs) are natural cyclic oligosaccharides industrially produced by the enzymatic digestion of starch. The most abundant α-, β- and γ-CDs are built of six, seven and eight glucose (D-(+)-glycopyranosyl) units, respectively, which are linked by α-1,4-glycosidic bonds. They possess a truncated cone shape with the primary and secondary hydroxyl groups located at the narrower and wider rims. Consequently, the molecules exhibit a hydrophilic exterior and a hydrophobic cavity due to the inward directed H3 and H5 atoms of the glucose unit (Fig. 1).[1]

CDs are known to form inclusion complexes, which is exploited in numerous applications, mainly in the pharmaceutical, cosmetic and nutritional fields.[2] Their cyclic structure, together with their

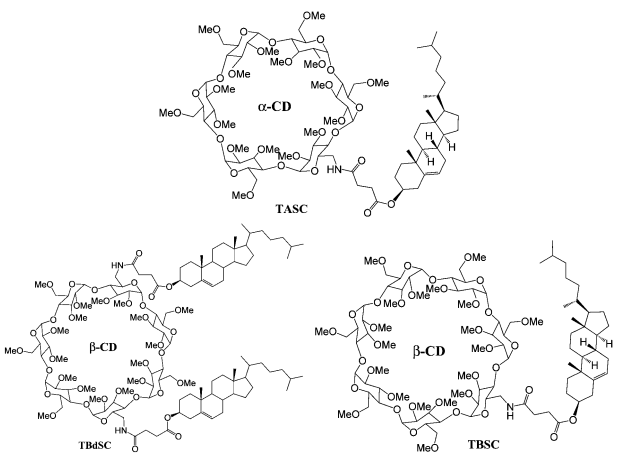

Fig. 1 Chemical structures of TASC, which is an abbreviation for the trivial name **T**rimethyl-**A**lpha-CD-**S**uccinyl-**C**holesterol; TBSC for **T**rimethyl-**B**eta-CD-**S**uccinyl-**C**holesterol and TBdSC for **T**rimethyl-**B**eta-CD-**di**S**uccinyl-**C**holesterol.

[a]*CEA, IRAMIS, SIS2M, LIONS, UMR 3299 CEA/CNRS, CEA-Saclay bât. 125, F-91191 Gif-sur-Yvette Cedex, France. E-mail: Jean.Daillant@cea.fr; Fax: (+33) 1 6908 6640; Tel: (+33) 1 6908 6481*
[b]*Université de Strasbourg, Institut Charles Sadron, CNRS, 23 Rue du Loess, BP 84047, 67034 Strasbourg Cedex 2, France*
[c]*Institut Laue-Langevin, 6 rue Jules Horowitz, BP 156, 38042 Grenoble Cedex, France*

† Electronic Supplementary Information (ESI) available: AFM and neutron reflectivity of the monolayer and bilayer and the structural parameter table. See DOI: 10.1039/c1sm06346d

readily modified hydroxyl groups, makes them convenient templates with a geometry defined by the chosen CD. The primary interest of modifying CDs is to tune their inclusion capacities and their solubility, as well as the solubility of their inclusion complexes. Furthermore, amphiphilic CDs have been designed in order to be able to control the supramolecular assemblies of CDs. But these modifications have mainly been restricted to uniformly functionalised or statistically described mixtures.[3] From a synthetic point of view, due to the large number of chemically equivalent OH-groups, the controlled modification, *e.g.* of one or two defined hydroxyl groups, is much more challenging. Today, methods have been developed allowing for the easy access to defined permethylated 6-monosubstituted, as well as 6A,6D-bisubstituted-diamino-CDs so that pure amphiphilic mono- and di-substituted CDs can be obtained. Recently, we described the synthesis of new amphiphilic CD derivatives (Fig. 1), such as TASC, which is composed of a hydrophilic permethylated α-CD part to which a hydrophobic cholesteryl residue is attached by a succinyl linker,[4] as well as TBSC and TBdSC, which are the permethylated mono- and di-substituted cholesteryl β-CD analogues of TASC.[5] Cholesterol has been proven to be an efficient membrane anchor. Two substitutions should even allow for double insertion and, thus, an increase in the anchoring strength. Using a succinyl spacer to attach cholesterol to the CD should still be short enough to avoid forming self-inclusion complexes simultaneously, whilst retaining sufficient flexibility.[6] Previous studies demonstrated that for all three investigated CDs, stable monolayers of the pure compounds can be obtained.[5,7] We thoroughly studied and compared their amphiphilic behavior and demonstrate that the CD head adjusts its conformation according to the available area per molecule.[4,5,7] Furthermore, insertion of TBdSC into the phospholipid model membranes[7] and phase separation has been shown, similar to the native monocholesteryl CDs.[6,8]

In this paper, we fully describe the interfacial behavior of DPPC mixtures with the amphiphilic CDs, TASC, TBSC and TBdSC, to achieve a complete understanding of the CD insertion properties from a macroscopic to a molecular level, with a special emphasis on the insertion behavior on the molecular scale. By calculating the inverse compressibility modulus and free excess Gibbs energy from the Langmuir isotherms, the influence of the CD ratio, CD type and the number of cholesteryl anchors on the membrane properties has been established. For TASC, the in-plane structure is characterised, on all scales, by Brewster angle microscopy (BAM) at the air–water interface and atomic force microscopy (AFM) of the mono- and bi-layers deposited on mica. Similar to TBdSC, TASC is miscible with the fluid DPPC phase, whereas demixing is observed for the gel phase of DPPC at high surface pressures. Furthermore, we studied the structure of mixed TASC/DPPC mono- and bi-layers perpendicular to the surface with Ångstrom resolution by neutron reflectivity. In this way a molecular model of the insertion has been established, which suggests that the CD cavities partly protrude into the subphase leaving them accessible for complex formation.

2 Experimental section

2.1 Used chemicals

The amphiphilic CDs were synthesised in our group. TASC 6^{I}-(α-cholesteryl) succinylamido-(6-deoxy-per-(2,3,6-*O*-methyl)) cyclohexaose was prepared as described recently.[4] The two β-CD derivatives, $6^{I},6^{IV}$-(β-cholesteryl) succinylamido-$6^{I},6^{IV}$-(6-deoxy-per-(2,3,6-*O*-methyl)) cycloheptaose (TBdSC) and 6^{I}-(α-cholesteryl) succinylamido-(6-deoxy-per-(2,3,6-*O*-methyl)) cycloheptaose (TBSC) were synthesised from permethylated amino-cyclodextrin.[5] DPPC (1,2-dipalmitoyl-*sn*-glycero-3-phosphocholine), chloroform (stabilized with ethanol) were purchased from Sigma–Aldrich. For the neutron reflectivity experiments, DPPC-d_{62} was bought from Avanti Polar Lipids and deuterium oxide (99.85% D, Euriso-Top) was provided by ILL. Ultra pure water (18.2 MΩ cm) was obtained from a Millipore purification system.

2.2 Langmuir isotherms

The surface pressure–area isotherms were measured with a temperature controlled Langmuir balance (702 BAM Film Balance for Brewster angle microscopy, Micro-Processor Interface IU4, NIMA Technology) used in conjunction with a BAM. Its maximum surface area was 700 cm^2, the minimum surface area was 80 cm^2 and it was filled with approximately 500 ml ultra pure water (18.2 MΩ cm) subphase. The trough, placed on an anti-vibration table, was covered by a plexiglas cover. The compounds were dissolved in chloroform and the solution was spread with a Hamilton syringe, typically using spreading volumes between 40 and 60 µl. The surface pressure, Π, was measured by the Wilhelmy plate method using filter paper. It is defined as

$$\Pi = \gamma_0 - \gamma \quad (1)$$

where γ_0 is the surface tension of the pure subphase and γ is the surface tension in the presence of amphiphiles at the interface. After 15 min of equilibration of the monolayer, the isotherms were recorded with a compression speed of 10 $cm^2\ min^{-1}$ at a temperature of 20 °C unless stated otherwise.

Isotherm analysis. In order to better identify the phase transitions in the isotherms, the derivative of the surface pressure, Π, with respect to the molecular area, A, has been determined from the isotherms to obtain the isothermal compressibility

$$C_S = -\frac{1}{A}\left(\frac{dA}{d\Pi}\right)_T. \quad (2)$$

It has been calculated numerically from the data as follows:

$$C_S = -\frac{1}{A_i}\frac{(A_{i+1} - A_i)}{(\Pi_{i+1} - \Pi_i)}. \quad (3)$$

A_i and Π_i are the molecular surface area and surface pressure corresponding to the data point, i, in the isotherm. For further analysis, we have taken the reciprocal isothermal compressibility to give the inverse compressibility modulus C_S^{-1}, which is a measure for interfacial elasticity. The smaller the C_S^{-1}, the higher the film elasticity.[9–11] For better visibility of the two-dimensional phase transition, the C_S^{-1} values were plotted in a log scale.

To find out about the mixing behavior, the excess free mixing energy ΔG_{mix}^{ex} was determined from the difference in work of the compression between the ideal and real mixed films, which can be

calculated by integrating the experimental Langmuir isotherms (4)

$$\Delta G_{\mathrm{mix}}^{\mathrm{ex}} = \int_0^{\Pi} [A - (x_1 A_1 + x_2 A_2)] \mathrm{d}\Pi, \quad (4)$$

where A is the molecular area for the binary mixture. A_n and x_n are the molecular area and molar fraction of the monolayer components.[12]

2.3 Brewster angle microscopy

The Brewster angle microscope (BAM, type PI, C-138K003, Optrel GBR, Berlin) co-aligned with the Langmuir trough was based on the Hoenig and Möbius setup.[13] A green laser (Las-Nova series 50) with a wavelength of 532 nm was directed onto the water surface at the Brewster angle (53.1°). The reflected light from the surface was imaged by means of a CCD camera (EHD®kamPro02) to give images of the monolayer morphology with a size of 480 μm × 599 μm and a resolution of 480 × 640 pixels.

2.4 Atomic force microscopy

Monolayers. Langmuir–Blodgett (LB) films of the monolayers were deposited onto hydrophilic, freshly cleaved mica wafers ($11 \times 11 \times 0.15$ mm^3, purchased from Agar Scientific) for several surface pressures from the air–water interface, with a dipping speed of 1 mm min^{-1}. Typically, for good monolayer depositions, transfer ratios close to 1 were obtained.

Bilayers. The bilayer samples were prepared like the monolayers with the Langmuir–Blodgett (LB) technique at $\pi =$ 40 mN m^{-1} and with a dipping speed of 1 mm min^{-1} for both layers. For the symmetrical bilayers, the first monolayer was deposited by lifting the wafer from the water and subsequently immersing the substrate into the water. For the asymmetrical bilayers, the water surface was thoroughly cleaned after the first deposition and a new monolayer was spread to deposit the second layer by immersing the wafer into the water. Then, the sample was carefully placed into a home-made teflon sample holder, which had been placed into the dipping well before hand in order to transport the sample under water. Typically, transfer ratios of 0.95 were obtained for both depositions.

Imaging. The films were examined with a Nanoscope V (Veeco) AFM in contact mode using cantilevers with a conical silicon etched probe tip (NSC19, MikroMasch) with spring constants in the order of 0.7 N m^{-1} for imaging the monolayers in air. For water imaging, triangular silicon nitride cantilevers with a reflective gold coating (DNP-S10, Veeco) and spring constants in the order of 0.06 N m^{-1} were utilised. The spring constants were verified prior to the experiments by the thermal resonance method.[14] Images with scan sizes ranging from 1 μm × 1 μm to 10 μm × 10 μm were recorded with scan rates of 0.5–1.5 Hz.

2.5 Neutron reflectivity

Monolayers. Two mixtures with 20 mol% TASC content were prepared: the first one using hydrogenated DPPC and a second one using deuterated DPPC-d_{62}. The CD/phospholipid samples, dissolved in chloroform, were spread in a Langmuir trough, which was perfectly aligned with the neutron beam. It was filled with a D_2O subphase and sealed with a Plexiglas cover. For both experiments the spreading volume was 90 μl. The chloroform was allowed to evaporate for 15 min. Then, the film was compressed at the desired surface pressure and the reflectivity curve was recorded.

The neutron reflectivity experiments at the air–liquid interface were carried out on a time-of-flight reflectometer (FIGARO, fluid interfaces grazing angles reflectometer) at the ILL, Grenoble.[15,16] The incoming beam comprised wavelengths between 2 Å and 30 Å and two incident angles ($\theta_1 = 0.62°$ and $\theta_2 = 3.82°$) were used. We could achieve a q-range from 0.005–0.35 Å^{-1} with resolutions determined by the chopper openings to be $\Delta q/q \sim$ 6.5% for θ_1 and $\Delta q/q \sim 8.6\%$ for θ_2. For details on the variable resolution options of the two instruments please see ref. 15 and 16. The samples were measured in a Langmuir trough (Nima), which was filled with the subphase. Its maximum and minimum areas were 930 cm^2 and 254 cm^2, respectively. The reflectivity was normalised by direct beams in a transmission geometry through the windows of the Langmuir trough lid and corrected for the incoherent background scattering.

Bilayers. The bilayers were prepared on $5 \times 5 \times 1$ cm^3 homogeneously n-doped silicon single crystals, oriented [111] on the side where the film was deposited and were atomically smooth with a roughness <5 Å, as determined by the manufacturer (SILTRONIX, Archamps, France). Prior to each deposition, the silicon block was cleaned with chloroform, ethanol and water then treated with UV/ozone for 30 min to reach a hydrophilicity as high as possible. For all the bilayers, deuterated DPPC-d_{62} was used.

The double layer deposition was carried out on a NIMA 611 trough available in the ILL soft matter lab (30×20 cm^2). The first layer was deposited by the classic Langmuir–Blodgett technique, whereas the second layer was deposited by the Langmuir–Schaefer method (the horizontal sample) at 40 mN m^{-1} and the temperature was kept constant at 20 °C. The samples were then inserted into a teflon sample cell, which was put into an aluminum box for mounting on the neutron reflectometer. The temperature was controlled using a water circulation bath. The cell was connected to a solvent circuit by means of a peristaltic pump in order to be able to change the subphase for different

Table 1 Selected SLDs for the used materials taken from ref. 4, 19 and 20

Material	SLD [10^{-6} Å^{-2}]
Si	2.07
SiO_2	3.47
D_2O	6.34
4MW	4.00
SMW	2.07
H_2O	−0.56
DPPC-palmitoyl tail	−0.41
DPPC-d_{62} palmitoyl tail	6.82
DPPC-PC head	1.74
TASC-CD head	2.15
TASC-cholesteryl tail	0.50

Table 2 The composition and contrasts used for the TASC/DPPC bilayers prepared for the neutron reflectivity experiment (sy: symmetric, as: asymmetric)

sample	1st layer	2nd layer	contrast
1 : 9 sy	10 mol% TASC	10 mol% TASC	D_2O, H_2O, SMW
2 : 8 as	Pure DPPC	20 mol% TASC	D_2O, SMW
5 : 5 as	Pure DPPC	50 mol% TASC	D_2O, 4MW, SMW

contrasts. More detailed information about the substrate and the sample preparation have been given elsewhere.[17] Symmetric bilayers, with the same composition for both leaflets, and asymmetric bilayers, with a first DPPC monolayer close to the silicon substrate and a second mixed layer exposed to the water subphase, were prepared (for details see Table 2).

The measurements were conducted on D17 reflectometer[18] operated in the time-of-flight mode at the ILL, Grenoble (France) with a wavelength range from 2 to 20 Å, giving a q-range for the specular reflectivity of 0.005–0.3 Å^{-1}. Each measurement was performed at two reflection angles, $\theta_1 = 0.8°$ (resolution: $\Delta q/q = 2.7\%$) and $\theta_2 = 3.2°$ (resolution: $\Delta q/q$ varied linearly from 3.8% to 13%).[18] The detector efficiency was calibrated with H_2O. For the actual experiment, the neutron beam entered the silicon substrate through one 5 × 1 cm^2 side of the block, hit the polished 5 × 5 cm^2 face on which the layer under study had been deposited at the grazing incidence, and exited through the opposite 5 × 1 cm^2 side.[17] Two direct beams have been measured at two angles of incidence for data normalization.

Different contrasts for various scattering length densities (SLD), such as H_2O (SLD = -0.56×10^{-6} Å^{-2}), silicon match water (SMW; SLD = 2.07×10^{-6} Å^{-2}), 4 match water (4MW, SLD = 4.0×10^{-6} Å^{-2}) and D_2O (SLD = 6.34×10^{-6} Å^{-2}) have been measured to remove the ambiguities of the fit (see Table 2).

Furthermore, for all the samples, at least one measurement has been done for the bilayer in the gel phase at 25 °C and in the liquid phase at 55 °C, which was monitored with a thermocouple (equilibration time: 25 min, stability: <0.1 °C, absolute precision: <0.3 °C) in the water-regulated sample chamber described in ref. 17. For annealing, one heating and cooling cycle was performed prior to the actual measurement. For two of the samples the intermediate temperatures, in steps of 5 °C, have also been measured.

Data analysis. Specular reflectivity, $R(q)$, is defined as the ratio between the specularly reflected and incoming intensities of a neutron beam, which is measured as a function of the wave vector transfer ($q = 4\pi/\lambda\sin\theta$) perpendicular to the reflecting surface, where θ is the angle and λ is the wavelength of the incoming beam. $R(q)$ is related to the scattering length density profile across the interface by the square modulus of its Fourier transform. Therefore, the phase is lost and the data needs to be fitted with an appropriate model to obtain the density profile. In this manner it is possible to determine the lipid film profiles with Å precision.[17,20] The data was fitted with the Motofit package run with the program IGOR Pro 6.0 (Wavemetrics, OR), where the specular reflectivity was calculated by the Abeles matrix method for stratified interfaces.[21] A detailed description of the Motofit software is given elsewhere.[22]

3 Results

3.1 Monolayers

Langmuir isotherms. Compression isotherms have been recorded for CD/DPPC mixtures with CD molar ratios between 0 and 100 mol% in steps of 10 mol% (Fig. 2 A–C). Mixed layers, containing TASC collapse independently from the mixing ratio at *ca.* 42 mN m^{-1} (Fig. 2 A). Using TBdSC, isotherms can be recorded up to surface pressures of even >50 mN m^{-1} (Fig. 2 C). The TBSC/DPPC isotherms can be compressed up to a plateau around 35 mN m^{-1}. For CD ratios smaller than 40% the films can be compressed further, up to surface pressures >50 mN m^{-1} (Fig. 2 B). At least for TBSC, it seems that the monolayers tend to get more stable with an increasing DPPC content and, if one considers the collapse pressure as a criterion for film stability, the TBdSC mixtures appear to be the most stable, followed by TASC and TBSC.[23] The greater stability of the TBdSC films might be caused by the stronger anchoring due to the two lipophilic cholesteryl anchors.

In order to better visualise the phase transitions in the isotherms, the data were plotted in terms of the surface pressure *vs.* the inverse isothermal compressibility (Fig. 2 D–F). The DPPC plateau (the first peak in the inverse compressibility plots) at 6 mN m^{-1}, which is assigned to the liquid expanded (LE)–liquid condensed (LC) phase transition, can only be found for mixtures with a CD content <20 mol%. However, it is less pronounced and shifted to higher surface pressures. The 10 mol% mixtures for TASC and TBdSC resemble DPPC also at high surface pressures (Fig. 2 D and F). Yet the maximum C_S^{-1} value is already greatly diminished compared to pure phosphocholine (250 mN m^{-1}), although it is still in the range of 100–250 mN m^{-1}, which is typical for the liquid condensed phase according to ref. 10. In contrast, TBSC already exhibits the features of pure CD (Fig. 2 E). For CD contents >50 mol%, the curves almost completely coincide with the ones of the pure CD (Fig. 2 E–F), with maximum values of C_S^{-1} in the order of 50–60 mN m^{-1}, which is similar to phospholipids in the liquid expanded phase at low surface pressures.[11,24]

At least for TASC and TBdSC, the CD's pseudo-plateau (the second peak in the inverse compressibility plots) is gradually shifted to higher surface pressures with decreasing CD content. This transition can most likely be assigned to a reorientation of the CD residues from a conformation where their cavities' axes are aligned perpendicular with respect to the interface to a conformation where it is aligned parallel with respect to the interface, as previously described for the pure methylated CDs.[4] The transition occurs at higher surface pressures with decreasing TASC content.

In order to gain a better understanding of the interactions between the phospholipid and the amphiphilic CDs, the excess free energy of mixing ΔG_{mix}^{ex} was calculated from the isotherms and plotted as a function of the molar fraction of the CD for the four different surface pressures (Fig. 3). Negative values indicate attractive interactions, whereas positive ones specify repulsive interactions. Due to rather large error bars for the calculations they can only be interpreted in a qualitative manner. All three different DPPC/CD mixtures are negative for low surface pressures and tend to get more positive with increasing surface

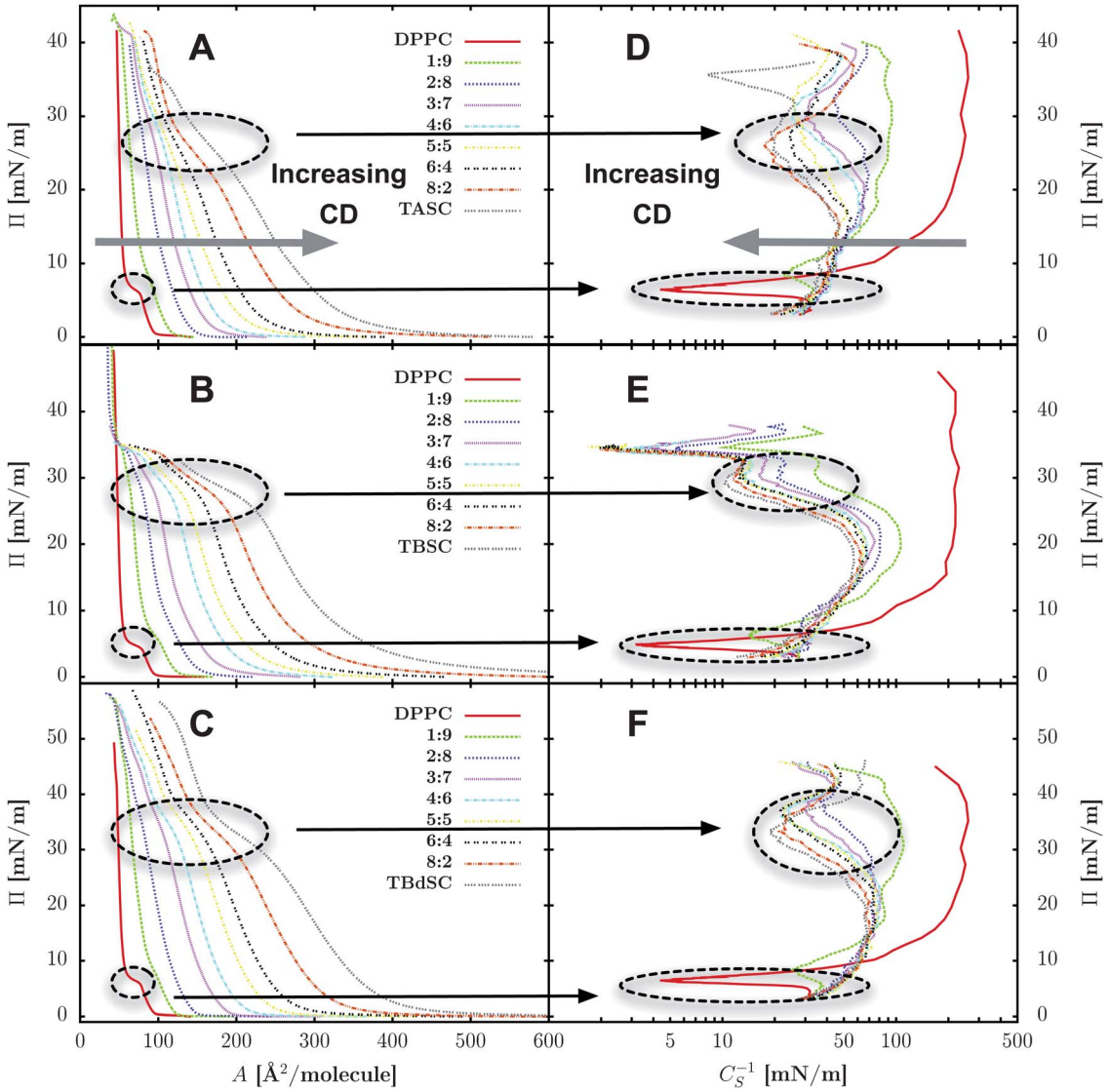

Fig. 2 Langmuir isotherms (left: A. TASC, B. TBSC, C. TBdSC) and inverse compressibility plots (right: D. TASC, E. TBSC, F. TBdSC) for CD/DPPC mixtures at 20 °C.

pressures. This means that the compounds get less miscible with compression. Looking at the general trend, the values for TBSC seem to be the most negative and the ones for TBdSC appear to be the most positive, leading to the assumption that the miscibility with DPPC decreases in the order: TBSC > TASC > TBdSC.

Monolayer in-plane morphology. With the help of BAM and AFM, the in-plane film morphology can be investigated from the μm to the nm scale. For low surface pressures, no contrast is observed with BAM (Fig. 4 A) and very flat AFM images without any features are obtained (Fig. 5 A). At 15 mN m^{-1}, bright domains appear (Fig. 4 B), which look like those for the liquid-expanded (LE) phase–liquid-condensed (LC) phase transition of pure DPPC.[25] Complementary AFM images (Fig. 5 B), show that the phase separation occurs also at smaller scales with small elevated zones of 30–80 nm diameter and a height <1 nm. With further compression the aggregates visible *via* BAM become less bright and denser; many of them consist of a bright core with dimmer surroundings (Fig. 4 C and D). These large domains are also visible in the AFM images and they possess a height of 1 nm (Fig. 5 C). The small aggregates, already visible for the lower compression, remain and, furthermore, there are now additional aggregates, which are 15–20 nm high. The friction contrast of the large domains is similar to the small ones already visible for 15 mN m^{-1}, whereas the tall aggregates, which appear for the high compression, are characterized by a very low friction (see the ESI†). Furthermore, it should be mentioned that the findings for the BAM and AFM are similar to what has been found for TBdSC/DPPC mixtures, except that there is no contrast inversion for the very high surface pressures.[7]

Monolayer structure perpendicular to the surface. Neutron reflectivity experiments were carried out to determine the film thickness and SLD profiles of the mixed CD/DPPC films for different surface pressures. In order to obtain a better contrast

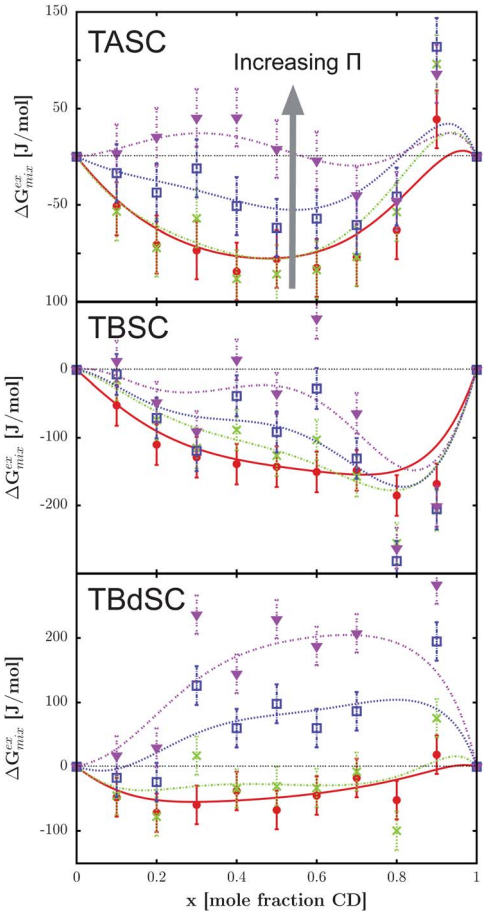

Fig. 3 ΔG^{ex}_{mix} *vs.* the molar fraction of the CD for different surface pressures from top to bottom A. TASC (●) 5 mN m^{-1}, (×) 15 mN m^{-1}, (□) 25 mN m^{-1}, (▼) 35 mN m^{-1}), B. TBSC (●) 5 mN m^{-1}, (×) 15 mN m^{-1}, (□) 25 mN m^{-1}, (▼) 33 mN m^{-1}) and C. TBdSC (●) 5 mN m^{-1}, (×) 15 mN m^{-1}, (□) 30 mN m^{-1}, (▼) 40 mN m^{-1}.

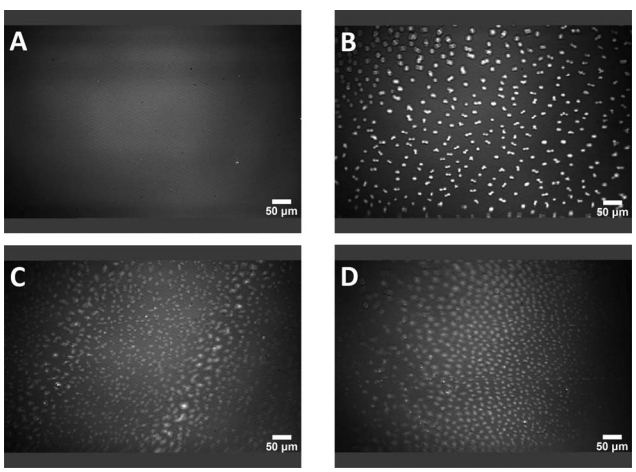

Fig. 4 BAM images for a DPPC monolayer with 20 mol% TASC, A. Π = 5 mN m^{-1}, B. Π = 15 mN m^{-1}, C. Π = 22 mN m^{-1}, D. Π = 35 mN m^{-1}.

and to avoid incoherent scattering, D_2O was used as a subphase for the neutron reflectivity measurements instead of normal water. The isotherms' shape was preserved, however, it is slightly

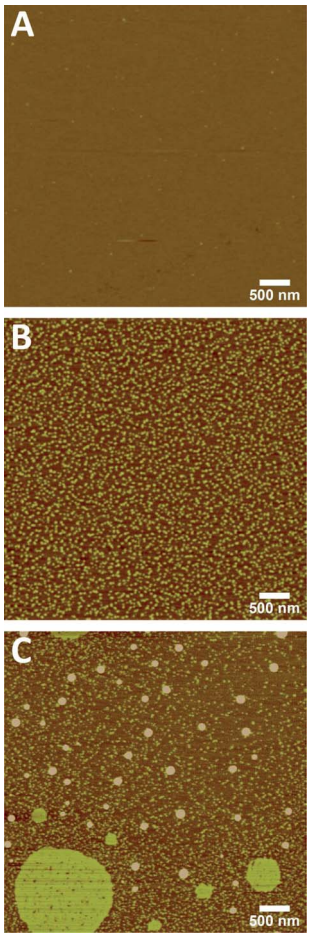

Fig. 5 AFM height images for a DPPC monolayer with 20 mol% TASC, A. Π = 5 mN m^{-1}, B. Π = 15 mN m^{-1}, C. Π = 35 mN m^{-1}.

shifted to higher molecular areas (~10 Å^2) compared to isotherms with a H_2O subphase, due to the isotope effect influencing the headgroups.[26]

The monolayer data (Fig. 6) was fitted using a two-layer box model with two distinct regions of scattering length densities and corresponding thicknesses. The top layer, which is close to the air, can be assigned to the hydrophobic tails of DPPC and the cholesteryl moieties of the CD, whereas the 2nd layer should consist of the hydrophilic DPPC head groups and CD residues. Furthermore, all roughnesses have been constrained to be the same for one surface pressure.

The reflectivity curves for TASC/DPPC-d_{62} in Fig. 6 clearly show a shift of the scattering curve minimum to lower q values with an increasing surface pressure, which indicates an increase in the monolayer thickness.

Expectedly, the total film thickness of the monolayer (Fig. 7, top) increases from ~16 Å to ~26 Å with the surface pressure. Also, the film roughness increases strongly from 1 Å to 4 Å for high compressions. Looking at the Π dependence of the SLD profile (Fig. 7, bottom), it reveals that there exists only a small SLD contrast between the hydrophilic and the hydrophobic slabs for the expanded monolayer.

The thickness of the hydrophilic layer increases from 8 Å at 5 mN m^{-1} to 12.5 Å at 40 mN m^{-1}, which is most pronounced

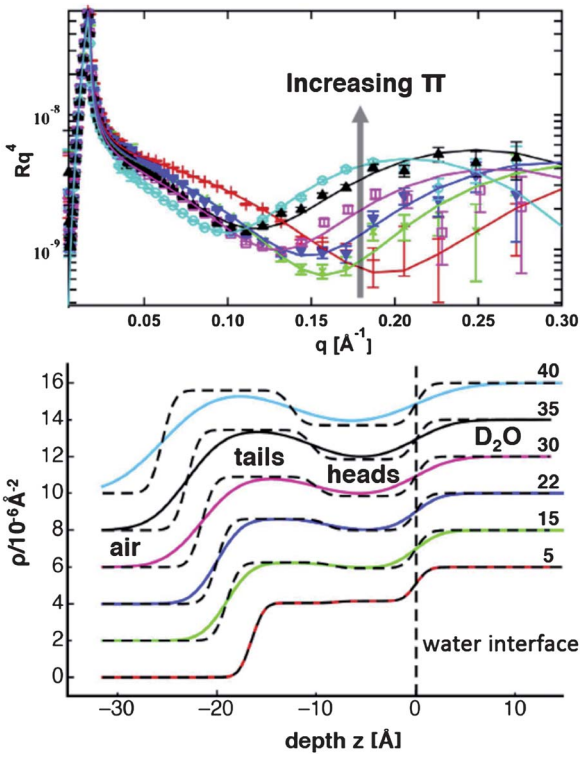

Fig. 6 Neutron reflectivity curves and SLD profiles, from bottom to top, with increasing surface pressures for TASC/DPPC-d_{62} 2 : 8 (+ is 5 mN m^{-1}, × is 15 mN m^{-1}, ▼ is 22 mN m^{-1}, □ is 30 mN m^{-1}, ▲ is 35 mN m^{-1} and ○ is 40 mN m^{-1}). The dashed lines in the SLD profile indicate the different slabs of the box model.

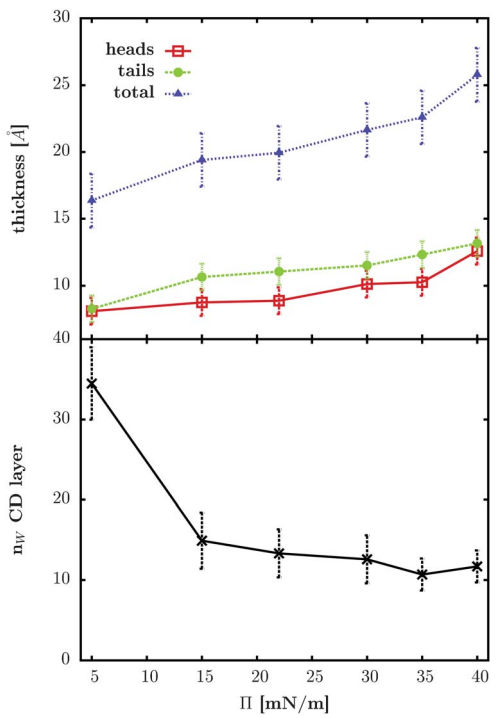

Fig. 7 Thickness of the TASC/DPPC monolayer (top) and the water content of the head layer (bottom) with changes in the surface pressure.

between 35 and 40 mN m^{-1}. It is accompanied by a drop in the SLD from 4.1 × 10^{-6} Å^{-2} to 3.7 × 10^{-6} Å^{-2} due to a loss of water (from 35 to 11 water molecules per headgroup). The number of water molecules was calculated in the same way as described in ref. 4.

The hydrophobic layer thickness increases from 8.3 Å at 5 mN m^{-1} to 13.2 Å at 40 mN m^{-1}, at which the tails contribute the most to the increase in the film thickness up to 15 mN m^{-1}. The maximum tail thickness is ~4 Å smaller than described for pure DPPC,[26,27] as well as the DPPC/cholesterol mixtures.[28] During compression, the SLD increased from 4.0 × 10^{-6} Å^{-2} to 5.6 × 10^{-6} Å^{-2} for deuterated DPPC and from −0.3 × 10^{-6} Å^{-2} to 0.25 × 10^{-6} Å^{-2} for the mixed layer containing hydrogenated DPPC (see Table 3 and Fig. 7), which indicates a more compact arrangement.

3.2 Bilayers

Bilayer in-plane morphology. The bilayers, which were deposited on mica substrates with the same compositions as those investigated by neutron reflectivity, were imaged by AFM in water (Fig. 8). All three studied bilayers are rather homogeneous and the phase separation is obvious, which is consistent with the findings for the monolayers at high surface pressures. The symmetric bilayer displays a height difference between the zones of ~1 nm compared to ~0.5 nm for the asymmetric ones. In addition, there are holes of ~5 nm in the 10 mol% TASC sample (Fig. 8 A), which correspond very well to the bilayer thickness. As observed for the monolayers, the friction is greater for the elevated domains (see ESI†). Comparing the asymmetric bilayers with 20 mol% and 50 mol% TASC, the elevated domains decrease with an increasing CD content, which leads to the conclusion that the domains mainly consist of DPPC.

Bilayer structure perpendicular to the surface. For symmetric bilayers, a 5 layer model was adopted with two headgroup slabs, an inner membrane layer for the hydrophobic part, a SiO_2 layer on the silicon block, as well as a thin water layer between the membrane and the substrate. For the asymmetric bilayer, a 6th layer was added to take into account that the inner membrane layer is divided in the slab, which consists only of DPPC tails and another one where the lipid chains are mixed with the cholesteryl residues of the CDs.

The fits for the different contrasts have been performed in a coupled manner. For the monolayer, only the SLD of the hydrophobic tails was allowed to vary for both contrasts. For the bilayers, only the subphase scattering length density was changed for the different contrasts. The error bars were determined by varying each parameter of the model and evaluating the χ^2 parameter, as well as visually checking the quality of the fit. The results fall within the error bars if they still give satisfactory fits for all measured contrasts. Concerning the measurements for temperatures in between 25 and 55 °C, where only one contrast has been measured, the same error bars have been adopted as those obtained for the samples measured with several contrasts.

Good coupled fits could be obtained for all the measured samples at different temperatures with an exploitable q-range from 0.01 to 0.25 Å^{-1}. Stable bilayers can be prepared for a symmetric bilayer, with both membrane leaflets containing

Table 3 Fitting results for the DPPC-d_{62} monolayer with 20 mol% TASC (Fig. 6 at different surface pressures). l_x is the thickness and SLD_x is the scattering length density of slab x

Π [mN m^{-1}]	l_{head} [Å]	SLD_{head} [10^{-6} Å^{-2}]	Water [%]	l_{tail} [Å]	SLD_{tail}-d_{62} [10^{-6} Å^{-2}]	SLD_{tail}-H [10^{-6} Å^{-2}]	Roughness [Å]
5	8.0	4.15	56	8.5	4.05	−0.30	1
15	8.5	3.95	52	10.5	4.25	−0.05	2
22	9.0	4.00	54	11.0	4.60	0.15	2
30	10.0	3.85	51	11.5	4.90	0.15	3
35	10.5	3.85	51	12.5	5.45	0.20	3
40	12.5	3.70	48	13.0	5.60	0.25	4
Errors:	±1	±0.2	±5	±1	±0.2	±0.2	±1

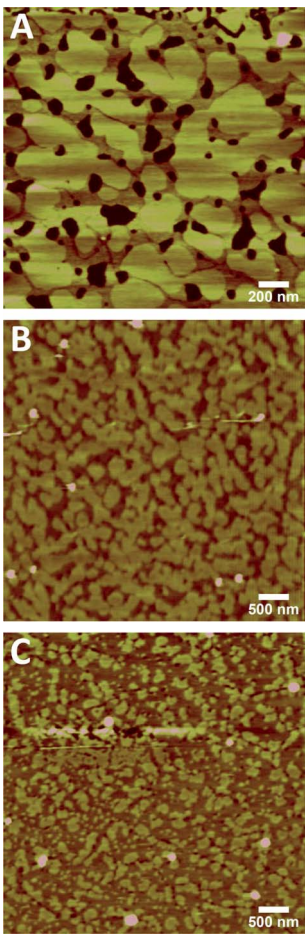

Fig. 8 AFM height images for TASC/DPPC bilayers deposited at 40 mN m^{-1}; A. symmetric 10 mol% TASC, B. asymmetric 20 mol% TASC, C. asymmetric 50 mol% TASC.

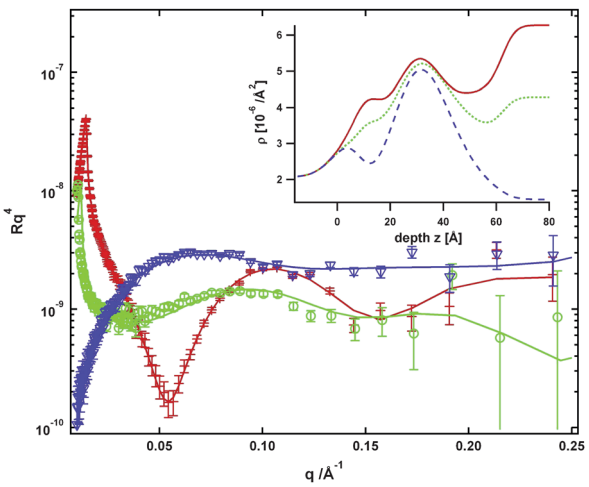

Fig. 9 Neutron reflectivity curves for the asymmetric bilayer with 50 mol % TASC at 55 °C recorded at three contrasts: H_2O (+), 4MW (○) and SMW (▽), as well as the corresponding SDL profiles for H_2O (—), 4MW (···) and SMW (–).

10 mol% TASC, as well as asymmetric bilayers with the outer layer containing up to 50% CD (Fig. 9; the reflectivity curves for the other samples, as well as the fitting results, can be found in the ESI†).

The silicon substrates were characterized first, and showed a SiO_2 layer, which was 8–11 Å thick with a roughness of ~5 Å. The parameters have been constrained to these values to fit the supported bilayer experiments. A water layer of 1.5–3.5 Å thickness with a roughness between 4–5 Å had to be systematically added between the substrate and the membrane for all the samples and temperatures. Compared to the symmetric bilayers, the water layer of the asymmetric ones was somewhat elevated (3–3.5 Å), but it was still smaller than what has been reported in the literature.[17,20] At least for the symmetric layer, due to the strong hydration and the high roughness between the layers, the interface may not be very well defined. Consequently, as the resolution limit of the experiment is reached, it becomes difficult to discern the water film from the headgroups.

The box-model for the symmetric bilayer contains two headgroup regions and one single central tail layer. For the asymmetric membranes, the latter is divided into a slab mainly containing DPPC tails and another slab consisting of mixed cholesterol and DPPC tails. For all the head and tail boxes, a roughness between 4–8 Å was found. This increases with temperature, which is very likely to be due to the stronger fluctuations of the membrane.[29]

The total bilayer thickness expands with the CD content and decreases with heating and it is several Å larger compared to the pure DPPC bilayers.[17,20] For the bilayer with 10 mol% TASC, the temperature-dependent decrease in the thickness (~4 Å) is less

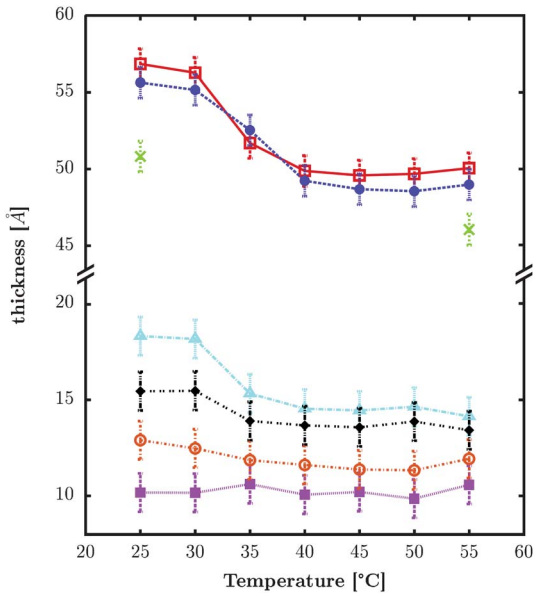

Fig. 10 Top: the total thickness as a function of the temperature for the symmetric bilayer containing 10 mol% TASC (×) and the asymmetric bilayers with 20 (●) and 50 mol% TASC content (□). Below: the temperature dependence of the thickness for the DPPC tail (▲) and the head group layer (■), as well as the mixed headgroup (◆) and tail layer (○) for the asymmetric 50 mol% TASC bilayer.

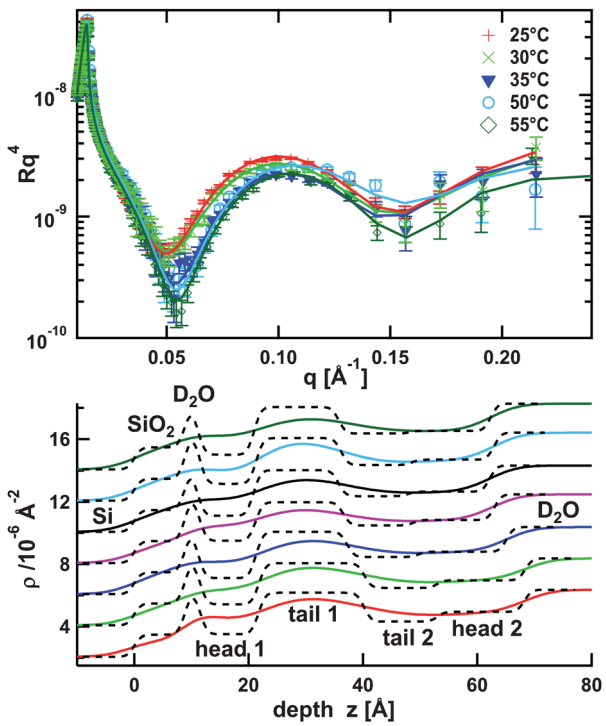

Fig. 11 Neutron reflectivity curves (for clarity, curves for 40 and 45 °C are not displayed) and SLD profiles for the asymmetric 50 mol% TASC bilayer as the temperature increases in steps of 5 °C from the bottom (25 °C) to the top (55 °C). The dashed lines in the SLD profile indicate the different slabs of the box model.

pronounced compared to the two asymmetric bilayers (~6 Å) (Fig. 10). For the asymmetric bilayers, the thickness obtained for the scattering curves taken at steps of 5 °C between 25 and 55 °C shows a drop in the thickness between 30–35 °C (which can be seen as two distinct populations in the scattering curves displayed in Fig. 11). This is due to the gel–liquid phase transition of the phospholipids, which is shifted compared to the main transition temperature of pure DPPC (~41 °C[30]). Moreover, due to the less ordered arrangement of the molecules in the liquid phase, the contrast between the tail and head slabs of the mixed layer decreases as the temperature increases (Fig. 11).

Looking at the mixed headgroup layers, an increase in the thickness and water content can be observed with a rising CD content and a decrease in the temperature. So, the water content for 20 mol% TASC decreases from 58% ($T = 25$ °C) to 51% ($T = 55$ °C) and, for 50 mol% TASC, it decreases from 68% ($T = 25$ °C) to 60% ($T = 55$ °C). In contrast, the headgroup's size and water content of pure DPPC (30–35%) in the asymmetric bilayer and the 10 mol% TASC symmetric bilayer show almost no temperature dependence. Furthermore, it seems that, for the symmetric bilayers, the headgroup slab that is close to the silicon substrate is marginally smaller and contains less water (30% close to substrate and 38% close to D_2O, see ESI† for details). Taking into account the molar ratios of the mixtures, the scattering length densities for the hydrophilic regions are in agreement with the values found in the literature for the pure compounds (Table 1). Consequently, the mixed head layer's SLD slightly increases with the CD content.

The tail layer gets thinner with an increasing CD ratio. A water content between 10–20% has been added to account for the holes. This is in agreement with what has been found in the literature.[31] Moreover, it is obvious that the temperature sensitivity of the thickness is significantly smaller compared to the pure DPPC tails when TASC is present in the membrane. The difference between 10 and 20 mol% TASC is very small, but is very likely to be due to the fact that it is difficult to compare the symmetric and asymmetric bilayers in a strictly quantitative manner. In order to compare the tail layer thickness of the symmetric sample with the asymmetric ones, it has been assumed that the tails of each monolayer contribute equally to the bilayer thickness. The points shown for 10 mol% TASC in Fig. 10 were obtained by dividing the thickness of the symmetric bilayer's tail slab by half. The scattering length densities of the hydrophobic membrane parts are consistent with values which can be found in the literature (Table 1). Consequently, the mixed tail layer's SLD decreases with a rising TASC content due to the higher cholesterol ratio.

4 Discussion

4.1 Miscibility and fluidizing effect of the cholesteryl CD

Previous studies with TBdSC at the air–water interface[7] and in multilamellar vesicles[5] show that it readily inserts into phospholipid membranes. Our results show that this is also the case for its mono-substituted cholesteryl α- and β-CD analogues since stable isotherms can be recorded for any kind of molar ratio.

ΔG^{ex}_{mix} calculations indicate a general demixing tendency of CDs and DPPC with increasing compression. Together with the

detailed study of the film morphology at various length scales for the α-CD analogue, the phase behavior of TASC/DPPC mixtures can be examined.

For low surface pressures, the two compounds are miscible and display a homogeneous in-plane structure at all scales. Similar to TBdSC, which is described in detail in ref. 7, at sufficiently high surface pressures, zones of DPPC in the condensed phase appear from which the CD is mostly expelled. Consequently, the phase surrounding these CD-depleted domains has to be enriched with CD. Yet, due to the fluidizing effect of the amphiphilic CDs, as mentioned previously, the liquid condensed phase starts to appear at much higher surface pressures than for pure DPPC.[25] This occurs at the μm scale (Fig. 4 B), as well as at the nanoscale (Fig. 5 B). With further compression (>30 mN m^{-1}), more and more condensed phase DPPC domains appear from which the CD can be expelled and these grow in size, sometimes around an aggregate core consisting of TASC (Fig. 4 C, D and 5 C). So, TASC mixtures behave in a very similar manner to TBdSC mixtures, except that there is no inversion of the contrast observed by BAM for surface pressures above 40 mN m^{-1}. This may be due to the fact that the film collapses before the α-CD residues can completely re-orientate.[7]

The $\Pi - C_S^{-1}$ behavior proves to be a useful tool to gain insight into the monolayer's 2D phase behavior. Caused by discontinuities in the lateral packing at the boundaries and the density fluctuations, a characteristic drop in C_S^{-1} for phase transitions can be detected.[11] A fluidizing effect of the amphiphilic CDs can be observed as the peak for the DPPC LE–LC co-existence region is shifted to higher surface pressures for a CD ratio of 10 mol%, which is similar to findings for cholesterol/DPPC films.[32] However, there is no strong condensing effect visible in the isotherms, which is usually typical for membranes containing sterols.[33] This is very likely due to the large CD moiety preventing close packing of the film.

The decrease in the inverse compressibility with cholesteryl CD contents until it matches those for pure CDs is in contrast to DPPC/cholesterol monolayers with sterol ratios larger than mol 10%[9] and can be explained by the great structural flexibility of the methylated CD moieties.[34,35] Due to their much larger size compared to the cholesteryl residue as well as the DPPC molecule, they dominate the properties of the mixed layers, rendering them almost as elastic as pure CD films.

4.2 Insertion of the cholesteryl CDs into membranes at the molecular level

Examining the surface pressure dependence of the mixed monolayer's SLD profile, it is evident that, for low surface pressures, almost no contrast between the head and tail layers exist; however, with further surface pressure increase a good contrast evolves (Fig. 6). This indicates a very disordered film structure for low compressions, which becomes more ordered at high surface pressures.

The hydrophobic tails contribute most to the increase in the film thickness up to 15 mN m^{-1} and can be attributed to the occurrence of DPPC in the LC phase. The sudden increase in the head layer thickness for high surface pressures (>30 mN m^{-1}) is probably related to an at least partial rearrangement of the CD moieties with respect to the interface.[4,7]

A decrease in the water content in the hydrophilic layer is observed with compression. It can be calculated from the SLDs and amounts to 35 water molecules per headgroup in the expanded state to 11 water molecules at a high compression (Fig. 7, bottom). Compared to pure DPPC headgroups,[27] where an expulsion of water from the headgroup layer is also observed, the number of water molecules in the mixed layer is significantly higher due to the strongly hydrated CD residues in the layer.[4]

The bilayers seem to get more difficult to prepare with increasing CD content since no stable bilayers could be obtained with TASC molar ratios exceeding 50% and in the AFM images defects are sometimes visible (*e.g.* Fig. 8 A). However, the studied bilayers are sufficiently stable to undergo the gel–liquid phase transition upon heating, which can be followed by looking at the evolution of the thickness with the temperature. The transition is shifted compared to pure DPPC from 41 °C[30] to temperatures between 30–35 °C. This is in agreement with the fluidizing effect already described for the monolayers, where the LE–LC phase transition is also shifted. Furthermore, the discrete partitioning between the DPPC layer and the mixed layer is preserved upon heating and cooling. This shows that there is no significant reorganisation of the asymmetric bilayer and no, or only very few, flip–flop events occur where the amphiphilic CD is exchanged between the leaflets.

When the layers contain TASC, the tail size remains almost unchanged during heating, which is in contrast to pure DPPC. This can be explained by the fluidizing effect of the CD since it is already in a very disordered state, even at low temperatures. The headgroup thickness, however, decreases significantly for the disordered liquid phase since, in this state, the 'soft' CD moiety can arrange more freely without being constrained by its hydrophobic cholesteryl anchor, which is tightly packed in the condensed phase. The smaller headgroup size may also be due to a smaller quantity of water being adsorbed in the layer at high temperatures. The large difference in the thickness between the two tail slabs for asymmetric bilayers is mainly attributed to the disordering effect of the CD in the outer mixed layer. Another contribution to the large size disparity might be the fact that the inner DPPC layer tends to be thicker as it is strongly adsorbed to the substrate and this allows for a more ordered structure.[29]

For the asymmetric bilayers especially, a very large water content was found and may not only be caused by the strong hydration of the CD heads. Defects in the supported bilayer probably also contribute to the high water content. This explanation is supported by AFM images, which show holes with a depth in the order of magnitude of the bilayer thickness. These defects are also reflected in the ~10% elevated water content of the supported bilayer compared to the corresponding monolayer with 20 mol% TASC, as well as in the necessity to add a similar water content to the tail slabs of the bilayers.

It is striking that, for the mixed leaflet of the 20 mol% asymmetric bilayer at 25 °C, very similar results are obtained compared to the monolayer at 40 mN m^{-1}, except for the lower water content of the latter. This is an indication that the insertion of the CD is similar for mono- and bi-layers. By comparing the

measured SLD profiles for the monolayers and bilayers with the calculated ones using the SLD profiles of the pure compounds, which are computed with the help of the literature values,[4,17,26,27] it is possible to deduce the molecular arrangement of the CDs with respect to the phospholipids in the film. The asymmetric bilayer's SLD profile, which was used to fit the real one, was calculated from a DPPC bilayer and a hypothetical bilayer consisting of a pure DPPC and a pure TASC layer, which, in reality, cannot be prepared. For the mixed monolayer, as well as the bilayer, a good match between the tail layers of the calculated and the real SLD profiles can only be achieved when shifting the pure TASC layer profile with respect to the pure DPPC profile by 8 Å and 4 Å, respectively, into the water subphase. This leads to a molecular model of the mixed films like that displayed in Fig. 12, where the CD moiety of TASC protrudes from the headgroup layer. However, it seems that in the case of the bilayer, the CD is more embedded in the film. This finding is further supported by the high roughnesses found for the bilayers and the monolayers at high surface pressures. Of course the fits give only a rather qualitative picture as, in producing the model curves, it is assumed that the mixtures show the same structural behavior as the pure compounds.

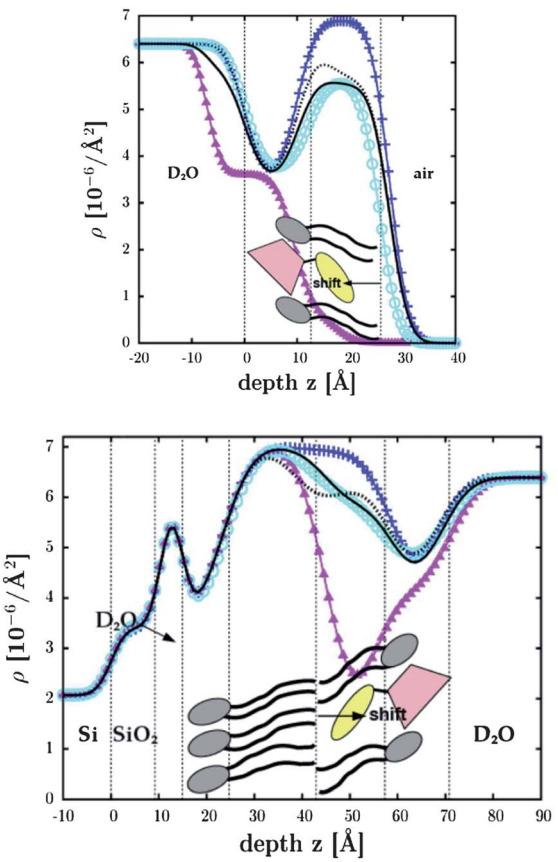

Fig. 12 A. Monolayer SLD profiles at 40 mN m^{-1} for pure DPPC (+), 20 mol% TASC (○) and pure TASC (▲). B. SLD profiles for the bilayer of pure DPPC (+), the asymmetric bilayer containing 20 mol% TASC (○) and the asymmetric bilayer containing pure TASC (▲) as an outer layer. In A. and B. the black and the dashed lines correspond to a model SLD profile for the 20 mol% TASC mixture calculated from the pure compounds with (—) and without shifting (···) the TASC layer towards the water interface.

5 Conclusions

A detailed understanding of the insertion behavior of amphiphilic cholesteryl CDs into phosholipid membranes has been achieved from the macroscopic to the molecular scale. Modified bilayers are stable and are subject to a gel–liquid phase transition upon heating. Depending on the compression, full miscibility of the two amphiphiles is observed for low Π and a clear demixing tendency is apparent during compression. Due to their bulky CD moiety, the amphiphilic CDs exhibit a distinct fluidizing effect on the membrane, which clearly renders it more elastic. TBdSC, with its two cholesteryl residues, seems to be best anchored to the membrane compared to its α- and β-CD analogues with only one membrane anchor. However, TASC appears to be more firmly inserted into the membrane than TBSC. With the help of neutron reflectivity, a molecular picture of the insertion has been achieved. At least for high surface pressures and temperatures below the gel–liquid phase transition, the CD residues partly protrude from the membrane, leaving the CD cavities accessible to form complexes.

Cholesteryl CDs appear to be suitable candidates as tools to functionalize natural membranes and synthetic vesicles. They are readily synthesized with cholesterol as stable and affordable anchors.[4,5] While being inserted into phospholipid membranes,[7] the conformational adaptability[4] and accessibility of the CD cavity prevails. This is crucial with respect to the CD's specific inclusion properties at the membrane surface and its pharmacological relevance regarding its use as a drug delivery vehicle, which should be addressed in future studies.[3,36] Since CDs are known to form rotaxanes with suitably sized polymers,[37,38] the cholesteryl CDs could serve as ideal compounds to bridge such supramolecular assemblies with macroscopic structures, like membranes. This could give rise to a new kind of sliding grafted polymer layer, which has been theoretically described by Baulin *et al.*[39] Subsequent studies are under way to design and characterize such topological grafts, where the connection between the different elements composing the material is defined by simple topological rules.

6 Acknowledgments

This work is supported by the French Research Program ANR-07-NANO-016-02 and Region Alsace (Ph.D. Grant). The authors wish to thank Carlos Marques from the ICS Strasbourg for the coordination of the ANR project and his kind support. We also wish to thank Maria Chiriac, Angelika Klaus, Mayeul Collot and Jean-Maurice Mallet for their intervention in the compound synthesis. Furthermore, we wish to thank the ILL for beam-time and the use of the PSCM facilities. We are grateful for the help and support of Hanna Wacklin and Richard Campbell during the neutron experiments on FIGARO and D17 at the ILL, Grenoble.

References

1 H. Dodziuk, *Cyclodextrins and their complexes*, WILEY-VCA, 2006.
2 J. Szejtli, *Chem. Rev.*, 1998, **98**, 1743–1753.
3 F. Sallas and R. Darcy, *Eur. J. Org. Chem.*, 2008, (6), 957–969.
4 M. Bauer, C. Fajolles, T. Charitat, H. Wacklin and J. Daillant, *Journal of Physical Chemistry B*, 2011, accepted.

5 M. Collot, M. Garcia-Moreno, C. Fajolles, M. Roux, L. Mauclaire and M.J., *Tetrahedron Lett.*, 2007, **48**, 8566–8569.
6 R. Auzely-Velty, B. Perly, O. Tache, T. Zemb, P. Jehan, P. Guenot, J. P. Dalbiez and F. Djedaini-Pilard, *Carbohydr. Res.*, 1999, **318**, 82–90.
7 A. Klaus, C. Fajolles, M. Bauer, M. Collot, J.-M. Mallet and J. Daillant, *Langmuir*, 2011, **27**, 7580–7586.
8 M. Roux, R. Auzely-Velty, F. Djedaini-Pilard and B. Perly, *Biophys. J.*, 2002, **82**, 813–822.
9 K. Sabatini, J. Mattila and K.K., *Biophys. J.*, 2008, **95**, 2340–2355.
10 J. Davies and E. Rideal, *Interfacial phenomena*, Academic Press, New York, 2nd edition, 1963, 265.
11 J. Smaby, V. Kulkarni, M. Momsen and R. Brown, *Biophys. J.*, 1996, **70**, 868–877.
12 F. Goodrich, *Proceedings of the 2nd International Congress on Surface Activity* (Academic Press, London), 1957, 85–91.
13 D. Hoenig and D. Möbius, *J. Phys. Chem.*, 1991, **95**, 4590.
14 R. Lévy and M. Maaloum, *Nanotechnology*, 2002, **13**, 33–37.
15 FIGARO, Reflectometer at the ILL, http://www.ill.eu/instruments-support/instruments-groups/instruments/figaro/.
16 R. A. Campbell, H. Wacklin, I. Sutton, R. Cubitt and G. Fragneto, *Focus Point Eur. Phys. J.*, 2011, in press.
17 T. Charitat, E. Bellet-Amalric, G. Fragneto and F. Graner, *Eur. Phys. J. B*, 1999, **8**, 583–593.
18 T. Cubitt and G. Fragneto, *Appl. Phys. A: Mater. Sci. Process.*, 2002, **74**, s329–331.
19 B. Stidder, G. Fragneto and S. Roser, *Langmuir*, 2005, **21**, 9187–9193.
20 B. Koenig, S. Kureger, W. Orts, F. Majkrzak, N. Berk, J. Silverton and K. Gawritsch, *Langmuir*, 1996, **12**, 1343–1350.
21 O. Heavens, *Optical Properites of Thin Films*, Butterworth, 1955.
22 A. Nelson, *J. Appl. Crystallogr.*, 2006, **39**, 273–276.
23 P. Dynarowicz-Latka and K. Hac-Wydro, *Colloids Surf., B*, 2004, **37**, 21–25.
24 S. Ali, J. Smaby, M. Momsen, H. Bockmann and R. Brown, *Biophys. J.*, 1998, **74**, 338–348.
25 J. Zhao, D. Vollhardt, G. Brezesinski, S. Siegel, W. J., J. Li and R. Miller, *Colloids Surf., A*, 2000, **171**, 175–184.
26 D. Vaknin, K. Kjaer, J. Als-Nielsen and M. Lösche, *Biophys. J.*, 1991, **59**, 1325–1332.
27 C. Naumann, T. Brumm, A. Rennie, J. Penfold and M. Bayerl, *Langmuir*, 1995, **11**, 3948–3952.
28 J. Wu, T. Lin, C. Yang, U. Jeng, H. Lee and M.-R. R. Shih, *Colloids Surf., A*, 2006, **284–285**, 103–108.
29 L. Malaquin, T. Charitat and J. Daillant, *Eur. Phys. J. E*, 2010, **31**, 285–301.
30 Z. Leonenko, E. Finot, T. Dahms and D. Cramb, *Biophys. J.*, 2004, **86**, 3783–3793.
31 G. Fragneto, F. Graner, T. Charitat, P. Dubos and E. Bellet-Amalric, *Langmuir*, 2000, **16**, 4581–4588.
32 K. Kim, C. Kim and Y. Byun, *Langmuir*, 2001, **17**, 5066–5070.
33 P. Quinn and C. Wolf, *Biochim. Biophys. Acta, Biomembr.*, 2009, **1788**, 33–46.
34 T. Steiner and W. Saenger, *Carbohydr. Res.*, 1996, **282**, 53–63.
35 M. Caira, S. Bourne, W. Mhlongo and P. Dean, *Chem. Commun.*, 2004, (19), 2216–2217.
36 T. Loftsson and D. Duchène, *Int. J. Pharm.*, 2007, **329**, 1–11.
37 A. Harada, *Coord. Chem. Rev.*, 1996, **148**, 115–133.
38 G. Wenz, B. H. Han and A. Muller, *Chem. Rev.*, 2006, **106**, 782–817.
39 V. A. Baulin, A. Johner and C. M. Marques, *Macromolecules*, 2005, **38**, 1434–1441.